Atmospheric Environment 246 (2021) 118081

Contents lists available at ScienceDirect

Atmospheric Environment

journal homepage: http://www.elsevier.com/locate/atmosenv

Wintertime aerosol optical properties in Lanzhou, Northwest China: Emphasis on the rapid increase of aerosol absorption under high particulate pollution

Xu Guan [a], Min Wang [a], Tao Du [a], Pengfei Tian [a,*], Naiyue Zhang [a], Jinsen Shi [a,b], Yi Chang [c], Lei Zhang [a,b], Min Zhang [a], Xin Song [a], Yijia Sun [a]

[a] Key Laboratory for Semi-Arid Climate Change of the Ministry of Education, College of Atmospheric Sciences, Lanzhou University, Lanzhou, 730000, China
[b] Collaborative Innovation Center for Western Ecological Safety, Lanzhou University, Lanzhou, 730000, China
[c] Gansu Province Environmental Monitoring Center, Lanzhou, 730020, China

HIGHLIGHTS

- Winter aerosol absorption increased under high particulate pollution in Lanzhou.
- Elemental carbon and fine soils accounted for most of the aerosol absorption.
- Radiative forcing efficiency was highly correlated with single scattering albedo.

ARTICLE INFO

Keywords:
Aerosol absorption
Single scattering albedo
Absorption coefficient reconstruction
Absorption ångström exponent

ABSTRACT

The evolution of aerosol absorption and the contribution of absorbing species under different severities of particulate pollution are poorly understood, though absorption is key in aerosol radiative forcing. To resolve the problems, aerosol absorbing properties from low to high particulate pollution were investigated by using intensive observations of aerosol optical properties in the winter of 2019–2020 in Lanzhou, Northwest China. The aerosol scattering coefficient increased linearly with increasing particulate matter <2.5 μm in diameter ($PM_{2.5}$) and the absorption coefficient increased more rapidly under higher particulate pollution, leading to rapid decline in single scattering albedo (SSA) and sharp increase in mass absorption efficiency of $PM_{2.5}$ ($MAE_{PM2.5}$). The SSA ($MAE_{PM2.5}$) decreased (increased) from 0.87 (0.76) in the lowest $PM_{2.5}$ bin to 0.82 (1.11) in the highest $PM_{2.5}$ bin. The linear relationship between the scattering coefficient and $PM_{2.5}$ was attributed to decreasing aerosol hygroscopicity with increasing $PM_{2.5}$. Elemental carbon (EC), fine soils (FS), and organic carbon (OC) accounted for 77.4%, 16.6%, and 6.0% of the total aerosol absorption, respectively. From low to high particulate pollution levels, the contribution of EC absorption increased from 68.3% to 80.5% while that of FS decreased from 25.5% to 13.9%. The aerosol radiative forcing efficiency was strongly correlated with SSA. Our results show a unique rapid increase in aerosol absorption under high particulate pollution during winter in Lanzhou, which is opposite to the trends observed in eastern Chinese cities, where SSA increases with increasing $PM_{2.5}$.

1. Introduction

Atmospheric aerosols impact the radiative budget of Earth's atmospheric system via aerosol–radiation and aerosol–cloud interactions (Twomey, 1977; Haywood and Ramaswamy, 1998; Bellouin et al., 2020). Absorbing aerosols play a unique role in aerosol–radiation interactions due to the heating effect in and at the top of the atmosphere (Jacobson, 2001). Specifically, absorbing aerosols deteriorate air quality (Ding et al., 2016; Zhang et al., 2020a), increase extreme weather (Fan et al., 2015), impact global and regional climate change (Bond et al., 2013), and damage human health (Janssen et al., 2011). Absorbing aerosols are increasingly of interest to researchers and policymakers (IPCC, 2013; Liu et al., 2020). Relevant emission reduction policies have been introduced for absorbing aerosols such as black carbon (Shindell

* Corresponding author.
E-mail address: tianpf@lzu.edu.cn (P. Tian).

https://doi.org/10.1016/j.atmosenv.2020.118081
Received 23 July 2020; Received in revised form 5 November 2020; Accepted 12 November 2020
Available online 17 November 2020

et al., 2012). However, assessing the radiative effects of absorbing aerosols remains challenging due to various reasons such as uncertainty of emission sources (Ferrero et al., 2018), complex optical properties (Andreae and Gelencser, 2006; Tian et al., 2018), methodological consistency and sophistication in observations (Yu et al., 2006; Barman et al., 2019), spatial and temporal variations (Kang et al., 2017), and poor parameterization in model simulations (Liu et al., 2017).

Absorbing aerosols heat the atmosphere and generally have a positive radiative force on the climate system. The global aerosol radiative absorption has been estimated to vary from 0.1 to 0.6 W m^{-2} (Allen et al., 2012; Myhre et al., 2013) to 0.9–1.2 W m^{-2} (Sato et al., 2003; Ramanathan and Carmichael, 2008). Black carbon (BC) is the major absorbing aerosol species (Bond et al., 2006; Cappa et al., 2012) and BC in polluted urban environments plays an essential role in pollution development and greatly contributes to large positive radiative forcing (Peng et al., 2016). Mineral dust and part of organic carbon (OC) are also absorbing aerosols in addition to BC. Mineral dust affects the radiation balance of Earth's atmospheric system via interactions with solar short-wave radiation and Earth's long-wave radiation (Miller and Tegen, 1998; Hu et al., 2019). It has been estimated that more than half of the absorption aerosol optical depth at 550 nm is derived from dust aerosols (Chin et al., 2009). Absorbing OC (or brown carbon, BrC) mainly originates from the combustion of coal and biomass and exhibits significant absorption at the ultraviolet or shorter wavelengths (Feng et al., 2013; Bergin et al., 2015). The contribution of BC to the absorption aerosol optical depth for carbonaceous aerosols is greater in urban sites than in the background areas, while the contribution of BrC is higher in background sites (Cho et al., 2019). It was found that the contribution of BrC to the total light absorption at 635 nm can be as much as 34% in Lanzhou (Zhang et al., 2019). However, our understanding of the contributions of BC, mineral dust, and OC to absorption under different severities of particulate pollution remains limited.

The fraction of aerosol species varies under different severities of particulate pollution, which leads to changing absorption in complex urban aerosols. The absorbing aerosols (i.e., BC, dust, and BrC) are mainly derived from primary emissions (Bond et al., 2006; Bergin et al., 2015; Hu et al., 2019), while secondarily generated aerosols (e.g., sulfate, nitrate, and ammonium) contribute greatly to light scattering (Liu et al., 2008; Tao et al., 2015). The aging of BC aerosols causes absorption enhancement due to the "lensing effect" (Jacobson, 2001). High relative humidity promotes aerosol hygroscopicity growth and aqueous chemical reactions (Svenningsson et al., 1992; Wang et al., 2016), which is favorable for light scattering enhancement (Titos et al., 2016; Zhao et al., 2019). Although the absorption of aerosols in East China has increased since 2013 (Tao et al., 2020), the variation in the aerosol absorption for different particulate pollution is still unknown. For example, the single scattering albedo (SSA) in Beijing decreased moderately from 0.82 in 2014 to 0.78 in 2016 (Wang et al., 2019) and also showed an increasing trend during pollution events (Yang et al., 2015). The average SSA was 0.91 under clean conditions and increased to 0.93 during polluted days in Wuhan (Liao et al., 2020). However, observations from Guangdong revealed that the SSA decreased from 0.93 to 0.91 with increasing particulate pollution (Kong et al., 2020). Single scattering albedo also varies among cities and seasons (Cao et al., 2012; Segura et al., 2016; Venter et al., 2020). Overall, the evolution of aerosol absorption under different severities of particulate pollution has been poorly quantified and the reasons for the existing discrepancies in aerosol absorption among the cities worldwide remain unclear.

The fraction of secondary inorganic aerosols has been observed to decrease with increasing particulate matter <2.5 μm in diameter ($PM_{2.5}$) in Lanzhou (Du et al., 2020), which is opposite to results in eastern Chinese cities, such as Beijing, where aerosol scattering coefficient exhibits an exponential growth with $PM_{2.5}$ due to high hygroscopicity and strong aqueous chemical reactions (Zhang et al., 2020b). Lanzhou is in a semi-arid region that is characterized by low relative humidity and weak aqueous chemical reactions during winter (Du et al., 2020), which is unfavorable for light scattering enhancement. Furthermore, emissions of absorbing aerosols, including elemental carbon (EC), mineral dust, and OC greatly contribute to aerosol absorption during winter. Thus, the evolution of aerosol absorption under different severities of particulate pollution and the contributions of absorbing species were investigated based on multiple observations of aerosol optical properties in the winter of 2019–2020 in Lanzhou. Firstly, the aerosol optical properties were overviewed and found that SSA is relatively low in Lanzhou when compared with eastern Chinese cities. Then the features of aerosol scattering and absorption from low to high particulate pollution and the contribution of aerosol species were studied and results showed that absorption under high particulate pollution increased rapidly. Finally, the influence of aerosol species on aerosol absorption during wintertime in Lanzhou was analyzed.

2. Data and methodology

2.1. Overview of data

Field measurements were performed from December 3, 2019 to February 4, 2020 at the Lanzhou Atmospheric Components Monitoring Superstation (LACMS; 36.05°N, 103.87°E, 1520 m a.s.l.), which is on the campus of Lanzhou University at downtown area of Lanzhou City. Multiple online instruments were deployed to continuously measure the concentrations of particulate matter (PM) of different sizes, aerosol optical properties, chemical compositions, gases, atmospheric visibility, and meteorological parameters. An overview of the instruments is provided in Table S1. Detailed introduction of the site is available elsewhere (Du et al., 2020).

A PM synchronous mixing monitor (5030i SHARP, Thermo Fisher, USA) was used to monitor the hourly mass concentrations of PM with an aerodynamic diameter of up to 1.0 μm (PM_1), 2.5 μm ($PM_{2.5}$), 10 μm (PM_{10}), and total suspended particles (TSP) with a flow rate of 1 $m^3 h^{-1}$. Aerosol scattering coefficients of $PM_{2.5}$ at 450, 520, and 700 nm wavelengths were observed by using a nephelometer (Aurora-3000, BMET Co., Ltd., China). An external heater was placed at the air sampling inlet of the nephelometer, which maintained the temperature of air samples between 50 °C and 60 °C. The nephelometer also contained an internal heater, which heated the incoming air samples when their relative humidity (RH) of the air samples exceeded 40%. The two heaters evaporated the water droplets and decreased the RH to <20% at the LACMS site, which was measured by an integrated humidity sensor and displayed on the main screen of the nephelometer.

An aethalometer (AE33, Magee Scientific, USA) with a $PM_{2.5}$ inlet was used to measure the aerosol light absorption coefficients at 370, 470, 520, 590, 660, 880, and 950 nm. The matrix scattering effect of the AE33 aethalometer filter was corrected using the matrix scattering effect correction coefficient, C = 1.39, provided in the instruction manual for the filter tape. The influence of RH on the absorption coefficient is discussed in the Supplementary Materials (Text S2 and Fig. S5). No relationship was found between the absorption coefficient and RH.

The hourly water-soluble inorganic ions (Cl^-, NO_3^-, SO_4^{2-}, NH_4^+, Na^+, K^+, Mg^{2+}, and Ca^{2+}) in $PM_{2.5}$ were measured using a Monitor for AeRosols and Gases in ambient Air (MARGA, Applikon Biotechnology B. V., The Netherlands), an advanced and widely used instrument worldwide (Brink et al., 2019). An online and continuous particulate carbon monitor (Model-4/OCEC (RT-4) Lab, Sunset Laboratory, Inc., USA) was used to measure the hourly OC and EC in $PM_{2.5}$. This OC/EC monitor adopts the thermal/optical method approved by National Institute for Occupational Safety and Health to measure OC and EC collected on a quartz filter membrane.

Concentrations of trace gases, including O_3, SO_2, NO, NO_2, and CO, were obtained at a resolution of 1 h using a set of online gas analyzers (49i, 43i, 42i, and 48i, respectively; Thermo Fisher Scientific, USA). Hourly meteorological parameters were collected using a meteorological sensor (FWS500, Fronttech, Ltd., China), including temperature,

RH, air pressure, wind direction and wind speed. Atmospheric visibility at 880 nm was measured using a visibility meter (DNQ-2, China).

To ensure the quality of the observation data, all instruments were installed and operated in strict accordance with their instruction manuals and were calibrated according to regulations on time. Details on the calibrations are available in Table S3.

To better understand the changes in the optical properties and chemical compositions of aerosols under different severities of particulate pollution, the observations were grouped using two methods. First, observations were grouped into low (daily $PM_{2.5} \leq 35$ μg m^{-3}), moderate ($35 <$ daily $PM_{2.5} \leq 75$ μg m^{-3}), and high (daily $PM_{2.5} \geq 75$ μg m^{-3}) pollution levels. Sample numbers of the low, moderate, and high PM levels accounted for 9.4%, 40.6%, and 50.0%, respectively of the total samples. We also divided the total samples into 10 bins from low to high particulate pollution, with each bin including 149 samples.

2.2. A brief introduction to aerosol optical parameters

Black carbon is the light-absorbing carbon measured by optical instruments (Petzold et al., 2013). Carbonaceous aerosols are divided into OC and EC components via chemical thermo-optical (or thermal) methods. In emissions inventories and climate science, BC is usually synonymous with EC (Cheng et al., 2011). In the present study, BC was used to describe optical performance, while EC was related to chemical species.

The aerosol absorption coefficient was calculated as follows:

$$\sigma_{ap} = [BC]_{\lambda} \times MAC_{\lambda} \quad (1)$$

where $[BC]_{\lambda}$ is the BC concentration and MAC_{λ} is the cross section of mass absorption. Unless otherwise specified, σ_{sp} is the scattering coefficient at 520 nm and σ_{sp} is the scattering coefficient at 520 nm. The SSA was calculated from σ_{ap} and σ_{sp} at 520 nm to be:

$$SSA = \sigma_{sp}/\sigma_{ext} = \sigma_{sp}/(\sigma_{sp} + \sigma_{ap}) \quad (2)$$

The scattering Ångström exponent (SAE) is a parameter related to aerosol size; it is relatively low for large particles and high for small particles and may be expressed as follows:

$$SAE = -\frac{\log(\sigma_{sp,\lambda_1}) - \log(\sigma_{sp,\lambda_2})}{\log(\lambda_1) - \log(\lambda_2)} \quad (3)$$

where $\lambda_1 = 520$ and $\lambda_2 = 450$ nm.

The aerosol absorption coefficient is expressed as:

$$\sigma_{ap}(\lambda) = k\lambda^{-AAE} \quad (4)$$

where k is a constant, $\sigma_{ap}(\lambda)$ is the absorption coefficient at wavelength λ, and AAE is absorption Ångström exponent. AAE was calculated via power-law fitting based on the absorption coefficients at 370, 470, 520, 590, 660, 880, and 950 nm wavelengths. The AAE is an indicator of the dominant light absorber in aerosols. The mass absorption efficiency of $PM_{2.5}$ ($MAE_{PM2.5}$) was calculated as the ratio of the absorption coefficient at 520 nm to the mass concentration of $PM_{2.5}$:

$$MAE_{PM_{2.5}} = \sigma_{ap}/PM_{2.5} \quad (5)$$

The mass scattering efficiency of $PM_{2.5}$ ($MSE_{PM2.5}$) was then calculated by replacing σ_{ap} at 520 nm in Equation (5) with σ_{sp} at 520 nm.

The atmospheric extinction coefficient ($\sigma_{ext}(RH)$) at 550 nm ($Mm \cdot m^{-1}$) was calculated based on the visibility (Vis) data as follows (Koschmieder, 1924; Yang et al., 2015):

$$\sigma_{ext}(RH) = \frac{3.912 \times 10^3}{Vis} \times \left(\frac{880}{550}\right) \quad (6)$$

The aerosol scattering coefficient at 550 nm ($\sigma_{sp}(RH)$) was calculated as follows:

$$\sigma_{sp}(RH) = \sigma_{ext}(RH) - \sigma_{ap} - \sigma_{ag} - \sigma_{sg} \quad (7)$$

where σ_{ap} is the absorption coefficient at 550 nm, which was calculated from the absorption coefficient at 520 nm by using Equation (4). The scattering coefficient (σ_{sg}) of the gases was assumed to be a constant of 10 Mm m^{-1} (Liu et al., 2008). The absorption coefficient of gases (σ_{ag}) was calculated using the experimental equation (Hodkinson, 1966):

$$\sigma_{ag} = [NO_2] \times 0.33 \quad (8)$$

where $[NO_2]$ is the unit of NO_2 (ppbv).

The ratio of the aerosol scattering coefficient at a given RH ($\sigma_{sp}(RH)$) to that under dry conditions ($\sigma_{sp}(dry)$) (Carrico et al., 2003; Liu et al., 2008):

$$f(RH) = \frac{\sigma_{sp}(RH)}{\sigma_{sp}(dry)} = \frac{\sigma_{ext}(RH) - \sigma_{ap} - \sigma_{ag} - \sigma_{sg}}{\sigma_{sp}(dry)} \quad (9)$$

where $\sigma_{sp}(RH)$ is calculated from Equation (7) and $\sigma_{sp}(dry)$ is the scattering coefficient 550 nm converted from the nephelometer observations at 520 nm using Equation (3).

The backscatter fraction, b, is defined as the ratio of backscatter to total scattering at 520 nm (Marshall et al., 1995):

$$b = \sigma_{bsp}/\sigma_{sp} \quad (10)$$

The value of b is high for small particles and low for large particles. The average up-scatter fraction, β, was calculated as follows (Delene and Ogren, 2002)

$$\beta = 0.0817 + 1.8495b - 2.9682b^2 \quad (11)$$

Furthermore, the aerosol radiative forcing efficiency was calculated as follows:

$$\frac{\Delta F}{\tau} = -DS_0T_{at}^2(1 - A_c)\omega_0\beta\left\{(1 - R_s)^2 - \left(\frac{2R_s}{\beta}\right)\left[\left(\frac{1}{\omega_0}\right) - 1\right]\right\} \quad (12)$$

where D is the fractional day length, S_0 is the solar constant, T_{at} is the atmospheric transmission, A_c is the fractional cloud amount, and R_s is the surface reflectance. The values of D, S_0, T_{at}, A_c, R_s were from Haywood and Shine (1995). Equation (12) has been widely used to assess the intrinsic radiative forcing efficiency of aerosols at the top of the atmosphere (e.g., Sheridan and Ogren, 1999; Virkkula et al., 2011; Hassan et al., 2015).

2.3. Reconstruction of light absorption and scattering coefficients

The light extinction can be expressed as the sum of light scattering by particles (σ_{sp}) and gases (σ_{sg}), and the absorption of particles (σ_{ap}) and gases (σ_{ag}). The revised Interagency Monitoring of Protected Visual Environments (IMPROVE) algorithm (Pitchford et al., 2007) was used to evaluate the effect of chemical species on aerosol light extinction. The algorithm is detailed in the Supplementary Materials (Text S1).

The $PM_{2.5}$ concentrations was reconstructed by the sum of organic matter (OM), $(NH_4)_2SO_4$, NH_4NO_3, EC, fine soil (FS), Na^+, and Cl^- to assess whether or not these chemical species were representative of the measured $PM_{2.5}$. A strong positive correlation ($R^2 = 0.93$) was found between the reconstructed and measured $PM_{2.5}$ (Fig. 1a), the regression coefficient was 0.82, indicating that the chemical species were representative of the measured $PM_{2.5}$. A strong positive correlation ($R^2 = 0.92$) was also found between the EC concentration from Sunset OC/EC monitor and concentration by the Magee Scientific AE33 monitor, even though EC was lower than BC (Fig. 1b). The underestimation of EC is further discussed in the Supplementary Materials (Text S3). Since the IMPROVE algorithm assumes that both sulfate and nitrate are present in the form of ammonium sulfate and ammonium nitrate, the presence of sulfate and nitrate in Lanzhou was tested (Fig. 1c). The slope of the linear regression was 1.04, which indicated that ammonium was the

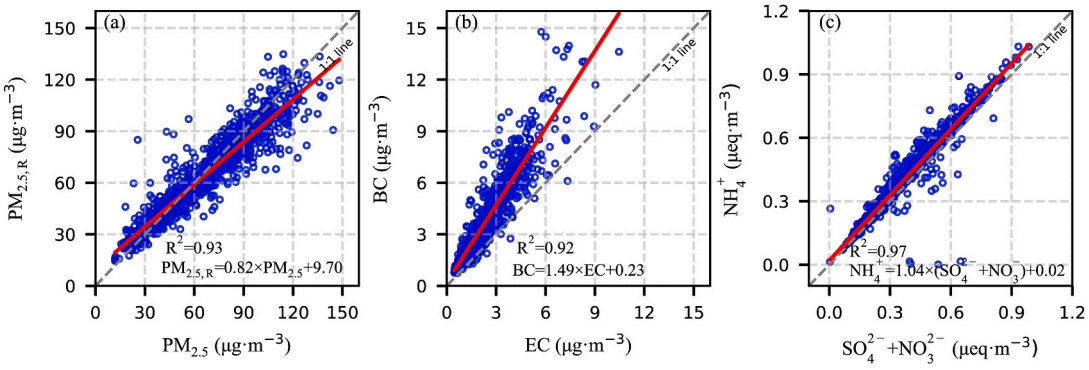

Fig. 1. Reconstruction of $PM_{2.5}$ (a), comparisons between EC and BC at 880 nm, and relationships between ammonium and the sum of sulfate and nitrate (c).

predominant forms of sulfate and nitrate.

The relationship between aerosol chemical species and optical parameters was studied to determine the influence of aerosol composition on optical properties. The scattering coefficient was most strongly correlated with OM and ammonium, followed by nitrate and sulfate (Fig. S2). A strong linear correlation ($R^2 = 0.93$) was observed between the absorption coefficient and EC (Fig. 2a) indicating that EC was the main species of absorption. The EC mass absorption coefficient at 520 nm calculated from the linear regression was 24.76 $m^2\ g^{-1}$, which was higher than that of 16.09 $m^2\ g^{-1}$ at 520 nm during summer in Beijing (Zhou et al., 2017). The high EC mass absorption coefficient may be due to deviations from different EC measurement protocols (Chow et al., 2004; Zhi et al., 2011) and the contribution of other absorbing chemical species in addition to EC (Yang et al., 2009).

Aerosol absorption and scattering were reconstructed to quantify the contributions of chemical species via the IMPROVE algorithm. The observed scattering coefficient was well represented by the IMPROVE method reconstructed scattering coefficient had a regression coefficient of 0.90 and a correlation coefficient of 0.86 (Fig. 2c). Aerosol non-sphericity is relatively high during winter in Lanzhou, indicating the presence of mineral dust aerosols (Tian et al., 2015). A stepwise multiple linear regression model (Chan et al., 1999) rather than IMPROVE was chosen to reconstruct the aerosol absorption coefficient because FS and absorbing OC contributed to aerosol absorption in addition to EC in

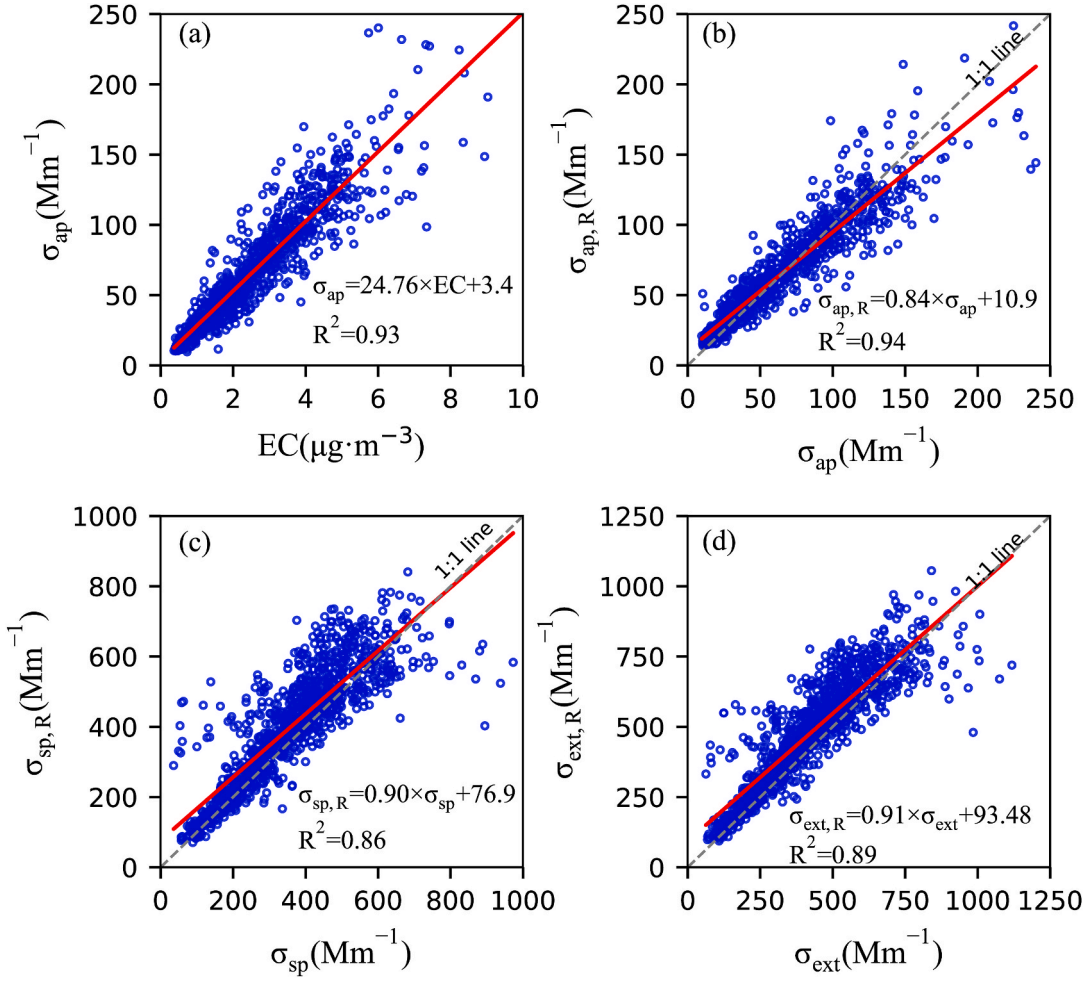

Fig. 2. Linear relationship between the measured b_{abs} and EC (a), the measured b_{abs}, b_{scat}, b_{ext} and the reconstructed b_{abs} (b), b_{scat} (c), and b_{ext} (d).

Lanzhou. The regression equation was established as follows:

$$b_{abs} = 21.2982 \times [EC] + 1.4065 \times [FS] + 0.2123 \times [OC] \quad (13)$$

The reconstructed absorption coefficient reasonably represented the observed absorption coefficient with a regression coefficient of 0.84 and a correlation coefficient of 0.94 (Fig. 2b). The regression coefficient and correlation coefficient between the reconstructed and observed extinction coefficient (i.e., the sum of scattering and absorption coefficient) were 0.91 and 0.89, respectively (Fig. 2d). Thus, the reconstruction method used in the present study is applicable in Lanzhou.

3. Results

3.1. Overview of aerosol optical properties during winter in Lanzhou

The aerosol optical parameters in the winter of 2019–2020 in Lanzhou were analyzed to better understand the aerosol optical properties in this region (Fig. 3). The range of the highest frequencies for σ_{ap}, σ_{sp}, and SSA were 15–30 Mm^{-1}, 350–400 Mm^{-1}, and 0.88–0.90, respectively. Single scattering albedos <0.7 were correlated with samples with high $\sigma_{ap} > 200$ Mm^{-1}. The average σ_{ap}, σ_{sp}, and SSA values were 64.70 Mm^{-1}, 363.68 Mm^{-1}, and 0.85, respectively (Table S2). Wintertime SSAs are relatively low in Lanzhou compared with eastern Chinese cities such as 0.94 for winter Hong Kong (Wang et al., 2017b), 0.89 for winter Nanjing (Zhuang et al., 2017), and 0.92 for hazy conditions during winter in Beijing (Zhang et al., 2020b).

The $MAE_{PM2.5}$ ($MSE_{PM2.5}$) ranged from 0.29 to 2.15 (0.55–8.78), with an average of 0.86 ± 0.31 (5.09 ± 0.70). Relatively high MAE further confirmed high absorption of atmospheric aerosols. AAE (SAE) ranged from 0.93 to 2.35 (0.31–3.89), with an average of 1.80 ± 0.18 (1.42 ± 0.28). The wide range of AAE and its average value of 1.80 indicated more other species in addition to BC aerosols. The aerosol hygroscopicity was very low (f(RH) = 1.68 ± 0.51), which might lead to different behavior of aerosol scattering coefficient as a function of PM against results in East China where aerosol scattering coefficient exhibits an exponentially growth with PM (Cheng et al., 2015; Ma et al., 2020). The $\Delta F/\tau$ was −22.58 ± 3.13 W m^{-2} in the winter of 2019–2020 in Lanzhou, the absolute value of which was less than that of −24.9 W m^{-2} in Nanjing (relatively heavily polluted site; Shen et al., 2018) and higher than that of −19.9 W m^{-2} in Finland (relatively clean site; Virkkula et al., 2011).

The scattering and absorption coefficients showed a clear double-

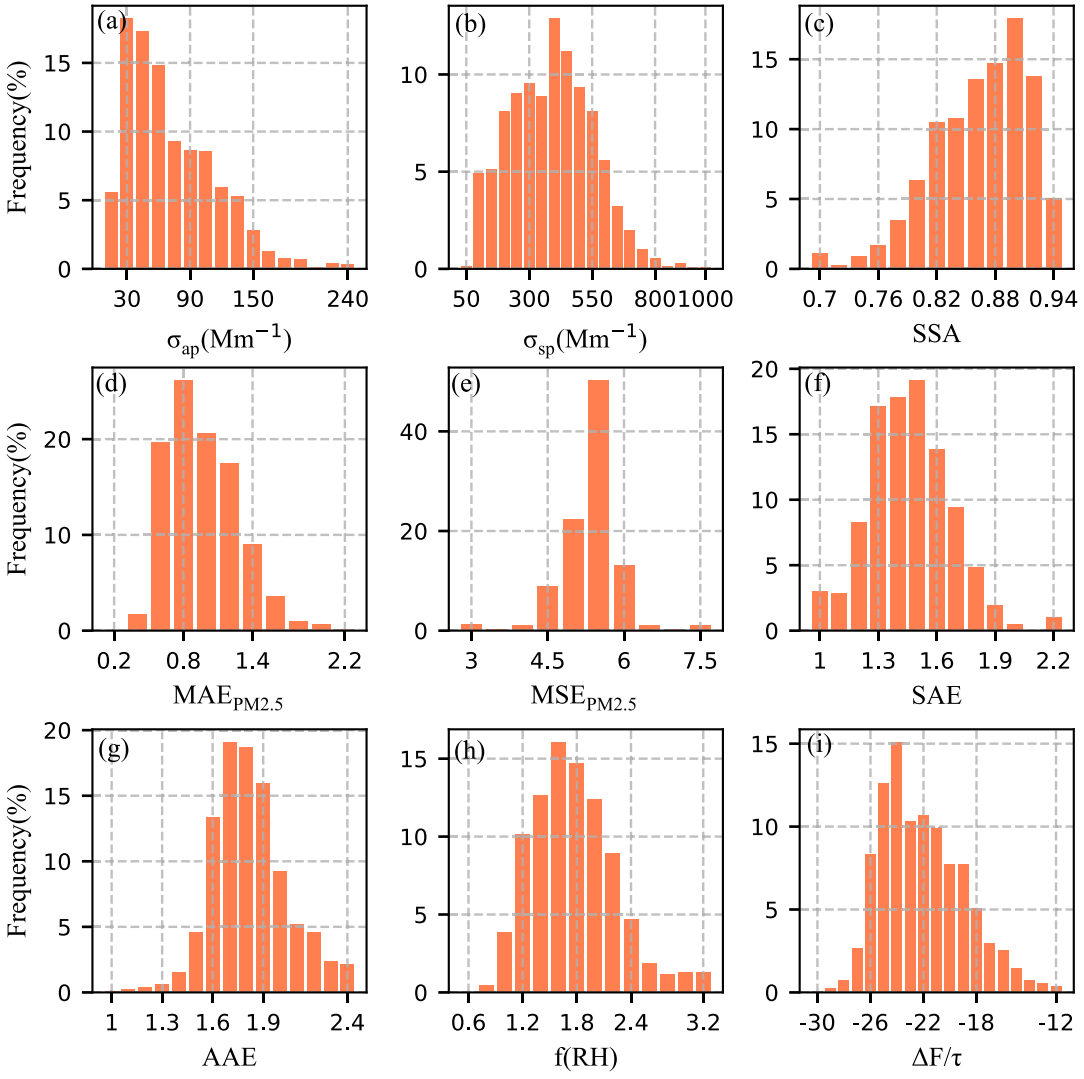

Fig. 3. Frequency distribution of aerosol optical parameters: (a) absorption coefficient, (b) scattering coefficient, (c) SSA, (d) mass absorption efficiency of $PM_{2.5}$, (e) mass scattering efficiency of $PM_{2.5}$, (f) scattering Ångström exponent, (g) absorbing Ångström exponent, (h) hygroscopic growth factor, and (i) radiative forcing efficiency in the winter of 2019–2020 in Lanzhou.

peaked diurnal variation, with the first peaks at noon (σ_{ap} at 11:00 and σ_{sp} at 13:00) and the second in the evening (20:00), and the first troughs before sunrise, with the second in the afternoon (Fig. 4a). The diurnal variation of $PM_{2.5}$ chemical species in the winter of 2019–2020 in Lanzhou has also been studied recently (Du et al., 2020), which provides information needed to explain the diurnal variation in the optical parameters. The first troughs resulted from a lack of photochemically generated aerosols (Zhang et al., 2017; Du et al., 2020) and continuous diffusion during the night while the second were caused by favorable diffusion conditions (i.e., deep boundary layer height and high wind speed; Fig. S4). Daytime anthropogenic emissions, photochemical generations, and increasing boundary layer heights (Xu et al., 2016; Tan et al., 2017; Du et al., 2020) led to the first peaks, while vehicle emissions during the evening rush hour and unfavorable diffusion conditions (i.e., shallow boundary layer height and low wind speed; Fig. S4) facilitated the second ones. The scattering and absorption coefficients began to increase at 07:00 due to daytime anthropogenic emissions. Meanwhile, the boundary layer height rapidly increased after 08:00, leading to favorable diffusion conditions around noon. The accumulation of anthropogenic emissions and increasing diffusion conditions jointly resulted in a peak in the aerosol absorption coefficient at 11:00, when the concentration of EC also peaked (Du et al., 2020). However, the scattering coefficient continued to increase until 13:00, indicating a high concentration of photochemically generated scattering secondary inorganic aerosols (SIAs) around noon. Both the scattering and absorption coefficients peaked at 20:00, which further demonstrated the contribution of photochemical generations for the first peak in the scattering coefficient.

Single scattering albedo ($MAE_{PM2.5}$) exhibited low (high) values during the absorption coefficient troughs. Smaller particles from photochemical generation during the day led to lower $MSE_{PM2.5}$ and higher SAE values during daytime. The diurnal variation of AAE was controlled by the aging of BC and changes in aerosol composition. Fresh BC in the late afternoon led to the lowest AAE at 19:00. Then aging of BC caused increasing trend in AAE until the next morning. Fresh BC emitted during the day led to a gradual decrease in AAE (see also Section 4.1). The diurnal variation of f(RH) was like that of RH (Fig. S1) but differed from that of the scattering coefficient, indicating the weak influence of humidity on aerosol scattering during winter in Lanzhou. The diurnal variation of $\Delta F/\tau$ was consistent with that of the absorption coefficient, which implied that aerosol radiative forcing was strongly influenced by absorbing aerosols.

3.2. Aerosol scattering and absorption from low to high particulate pollution

The scattering and absorption coefficients generally increased with increasing $PM_{2.5}$ in the winter of 2019–2020 in Lanzhou (Fig. 5a and b). The scattering coefficient exhibited a positive linear relationship with $PM_{2.5}$. However, the absorption coefficient showed two distinct linear relationships when $PM_{2.5}$ was either lower or higher than 69 μg m^{-3}. The absorption coefficient increased more rapidly with $PM_{2.5}$ under high particulate pollution conditions. The SSA remained stagnant when $PM_{2.5}$ was <69 μg m^{-3} but began to decrease rapidly with increases in $PM_{2.5}$ under high particulate pollution conditions (Fig. 5c). The SSA for the highest $PM_{2.5}$ bin reached as low as 0.82, which was lower than most cities in eastern China and globally under heavily polluted conditions such as 0.91 for Wuhan (Liao et al., 2020), 0.93 for Nanjing (Shen et al., 2018), 0.93 for Delhi (Tiwari et al., 2015), 0.91 for Finland, and 0.93 for Canada (Schmeisser et al., 2018). The $MAE_{PM2.5}$ showed little variation for the lowest four $PM_{2.5}$ bins but began to increase rapidly when $PM_{2.5}$ was higher than 69 μg m^{-3} (Fig. 5f). Rapid increase of aerosol absorption coefficient and mass absorption efficiency when $PM_{2.5}$ exceeded 69 μg m^{-3} seemed to be caused by the rapid increase of absorbing aerosols under high particulate pollution conditions (Fig. 6).

The scattering Ångström exponent exhibited little variation in the

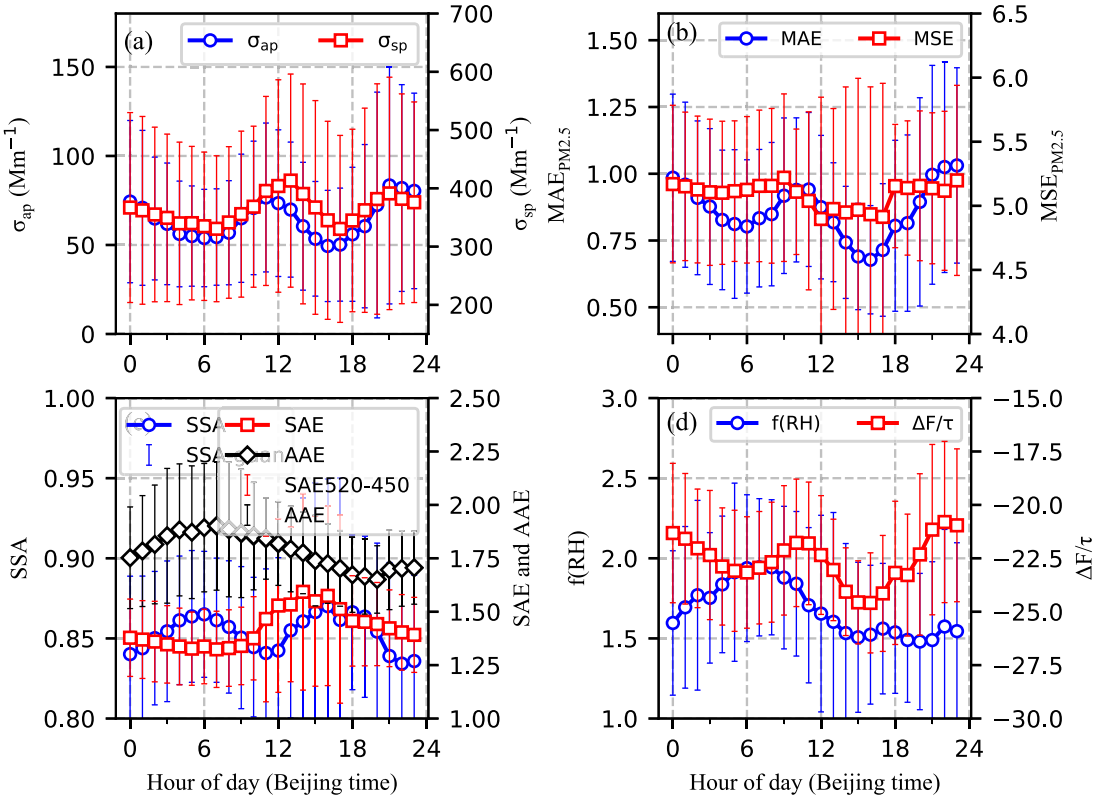

Fig. 4. Diurnal variation of aerosol optical parameters (a) absorption and scattering coefficients, (b) mass absorption and scattering efficiency of $PM_{2.5}$, (c) SSA and absorbing and scattering Ångström exponents, and (d) hygroscopic growth factor and radiative forcing efficiency.

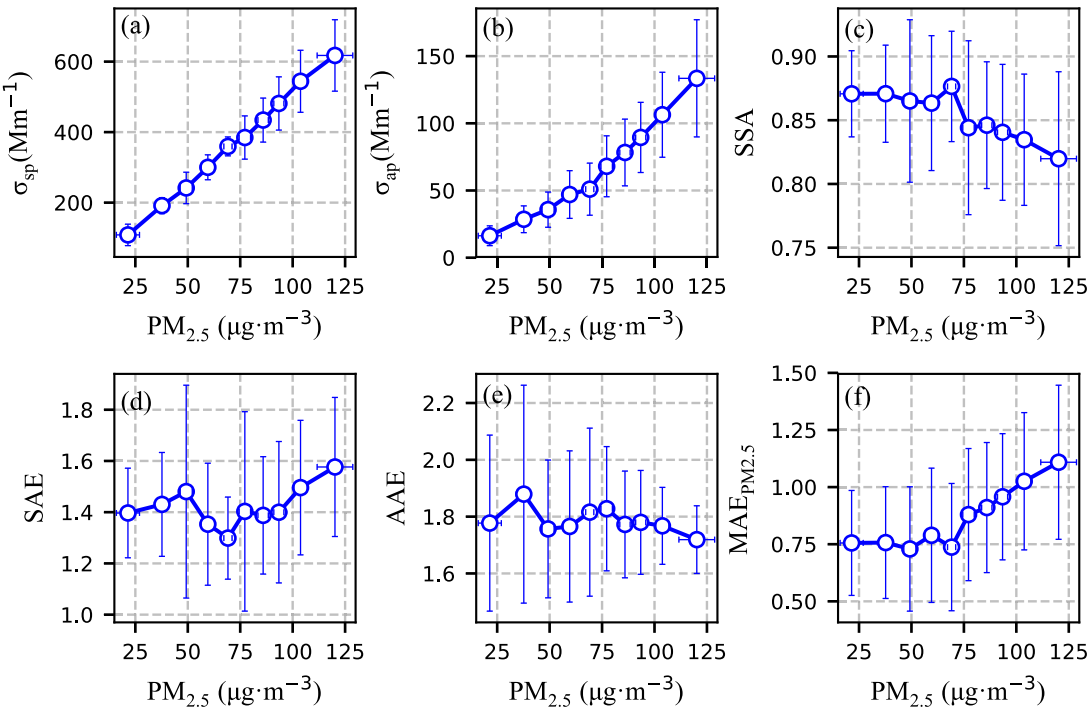

Fig. 5. Aerosol scattering and absorbing parameters as a function of $PM_{2.5}$: (a) scattering coefficient, (b) absorption coefficient, (c) SSA, (d) scattering Ångström exponent, (e) scattering Ångström exponent, and (f) mass absorption efficiency.

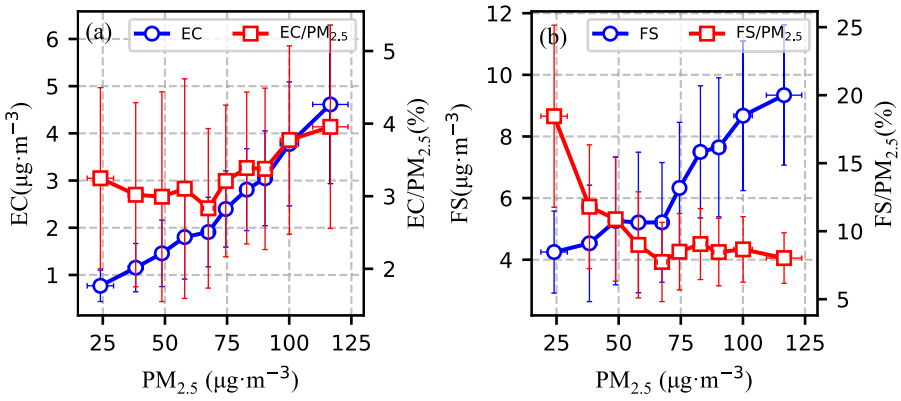

Fig. 6. Elemental carbon and the mass contribution of EC in $PM_{2.5}$ (a); FS and the mass contribution of FS in $PM_{2.5}$ (b) as a function of $PM_{2.5}$.

lowest four $PM_{2.5}$ bins but began to increase when $PM_{2.5}$ exceeded 69 μg m^{-3} (Fig. 5d), indicating increasing fine aerosols under high particulate pollution conditions. This phenomenon is opposite to that observed in eastern Chinese cities, where aerosols grow to larger size under polluted conditions due to aqueous reactions and hygroscopicity (Wang et al., 2016). In Lanzhou, the absorption Ångström exponent generally increased with $PM_{2.5}$ and began to decrease in the highest four $PM_{2.5}$ bins (Fig. 5e; see also Section 4.1).

The hygroscopicity of aerosols was investigated to better understand the aerosol scattering properties from low to high particulate pollution in the winter of 2019–2020 in Lanzhou. The correlation coefficient of the curve fitting relationship in Lanzhou City was as low as 0.65. The average RH was just 49.8% and RH rarely exceeded 80% during the winter of 2019–2020 in Lanzhou and such low humidity led to limited scattering enhancement of aerosols. The hygroscopic growth factor f (RH) decreased from 2.36 in the lowest $PM_{2.5}$ bin to 1.18 in the highest $PM_{2.5}$ bin, which was attributed to the relatively increasing hydrophobic OM and decreasing hydrophilic SIAs (Fig. 7b). In addition, the RH did not continue to increase with increases in particulate pollution (Fig. S3). Overall, the hygroscopic growth factor decreased with increases in $PM_{2.5}$, the weak influence of humidity on scattering led to an almost linear relationship between aerosol scattering coefficients and $PM_{2.5}$. This phenomenon is opposite to that recorded in eastern Chinese cities, where aerosol hygroscopicity and the generation of SIAs increase with increasing particulate pollution (Cheng et al., 2018; Wang et al., 2018; Ma et al., 2020) and SSA increases with increasing $PM_{2.5}$ (Zhang et al., 2020b).

3.3. The influence of aerosol composition on scattering and absorbing properties

The contribution of chemical species to aerosol extinction was studied using the reconstruction results (Fig. 8). The average reconstructed aerosol extinction coefficient was 475.0 Mm^{-1} and OM was the

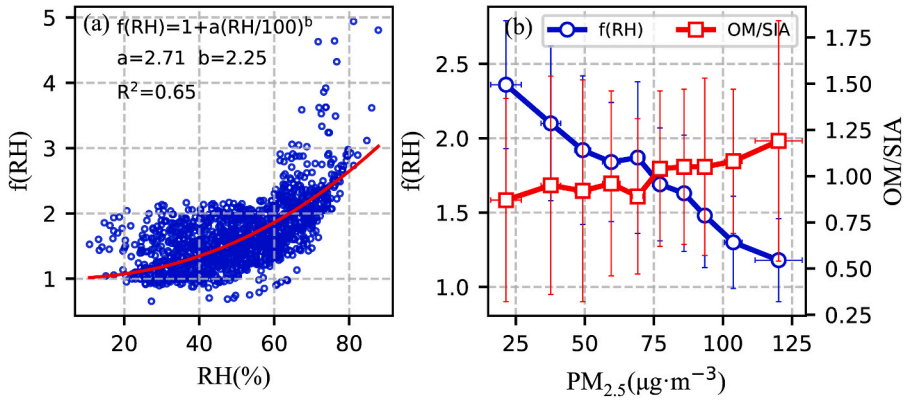

Fig. 7. Aerosol hygroscopicity as a function of RH (a) and $PM_{2.5}$ (b).

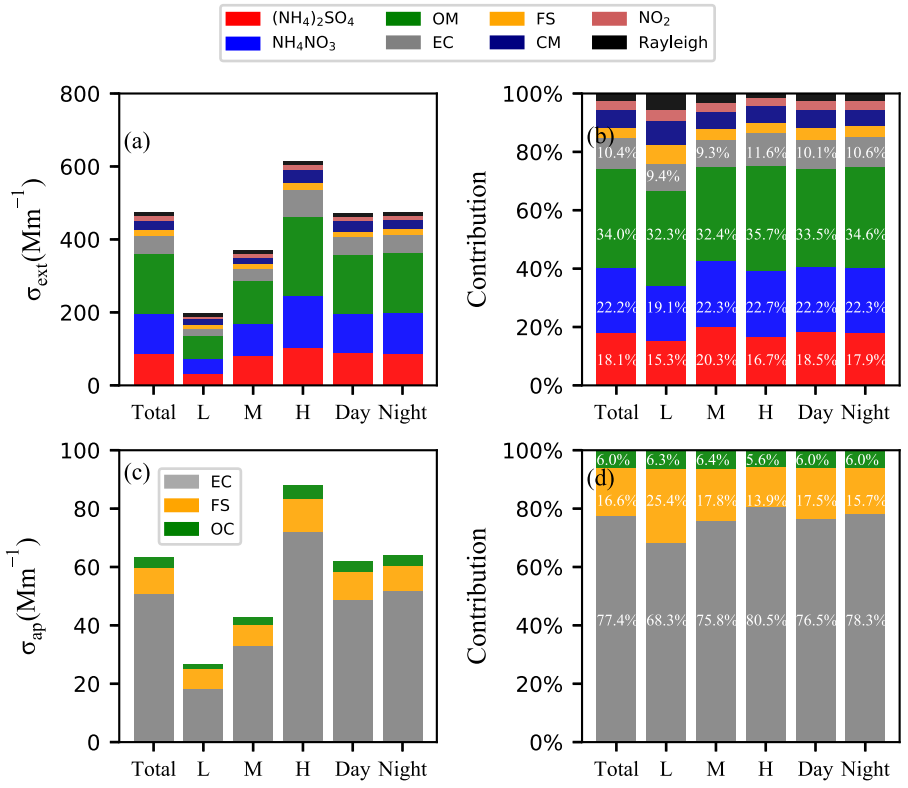

Fig. 8. Average compositions (left) and contributions (right) of aerosol extinction (upper) and absorption (lower) coefficients for total, low (L), moderate (M), and high (H) pollution levels, as well as daytime (08:00–19:00) and nighttime (00:00–07:00, 20:00–24:00) samples.

greatest contributor (34.0%), followed by ammonium nitrate (22.2%), ammonium sulfate (18.1%), EC (10.4%), and FS (3.7%). The contributions of OM, ammonium nitrate and EC increased from low (32.3%, 19.1%, and 9.4%) to high (35.7%, 22.7%, and 11.6%) pollution level, while the contribution of ammonium sulfate was the greatest for moderate level (20.3%).

The contributions of chemical species in Lanzhou to aerosol extinction were consistent with the results of some urban studies, such as in Beijing (Tao et al., 2015) and Shanghai (Han et al., 2015), where OM made the greatest contribution to extinction; the same conclusion was reached in Suzhou (Tian et al., 2016) for fine particles. Meanwhile the largest contributions of ammonium sulfate were found in Hainan (Tian et al., 2020), Guangzhou (Tao et al., 2014), and Xi'an (Cao et al., 2012).

The contributions of EC, FS, and OC on aerosol absorption were investigated in details (Fig. 8c and d). The average reconstructed aerosol absorption coefficient was 63.3 Mm^{-1} and the contributions of EC, FS, and OC were 77.4%, 16.6%, and 6.0%, respectively for total samples in the winter of 2019–2020 in Lanzhou. From low to high pollution levels, the contribution of EC absorption increased from 68.3% to 80.5%, while that of FS absorption decreased from 25.5% to 13.9%. The contribution of OC to aerosol absorption was minimal and exhibited little variation from low to high pollution levels.

4. Discussions

4.1. Combined effect of EC and FS on aerosol absorbing parameters

Single scattering albedo is a widely used parameter for aerosol absorption; the AAE is also an indicator of aerosol absorption. The AAE for fresh BC is ~1 (Bond and Bergstrom, 2006; Bond et al., 2013), while

those for other absorbing particles and BC coated by non-absorbing materials are >1 due to varying absorption in different wavelength range (Lack and Cappa, 2010; Valenzuela et al., 2015; Devi et al., 2016). For example, the AAE for mineral dust aerosols exceeds 2.0 (Weinzierl et al., 2011) and that for BrC can reach as high as 9.5 (Lack and Langridge, 2013). The AAE in the present study varied from 0.91 to 2.92, with an average of 1.80 (Fig. 9). Overall, the SSA was the highest when the EC/$PM_{2.5}$ mass fraction was the lowest and AAE had the widest range of variations under this situation. With the increase of EC/$PM_{2.5}$, SSA decreased to below 0.80 and the range of AAE narrowed, converging to ~1.65.

Three parts of the SSA–AAE plots were selected to better understand aerosol optical properties during winter in Lanzhou: (A) the upper left with AAE<1.63 and SSA>0.85, (B) AAE>1.96 and SSA>0.85, and (C) SSA<0.80. The sample numbers for parts A, B, and C were 194, 184, and 207, respectively. Part A of the SSA–AAE plots exhibited high SSAs and low AAEs. NH_4NO_3 accounted for the highest fraction (33.4%) of extinction for part A, followed by $(NH_4)_2SO_4$ (28.9%), and OM (21.1%). Both SSA and AAE were high in part B. The highest three extinction contributors were OM (38.7%), $(NH_4)_2SO_4$ (23.1%), and NH_4NO_3 (16.5%). Part C was characterized by low SSAs and medium AAEs. Organic matter contributed most to extinction (41.4%), followed by NH_4NO_3 (16.5%), and EC (15.6%). Relatively, part A was the cleanest and part C was the most polluted condition. There seems to be a gradual transition, first from A to B and then from B to C.

Elemental carbon and FS were the dominant species of aerosol absorption. The relatively low AAE and high SSA in part A were attributed to the low EC/$PM_{2.5}$ ratio. From part A to B, the contribution of FS (OM) increased more rapidly than that of EC, leading to an evident increase in the AAE and slight decrease in the SSA. From part B to C, the rapid increase in the contribution of EC, 8.4%–15.6%, led to a large decrease in both the SSA and AAE. Since EC accounted for 77.4% of the aerosol absorption during the winter of 2019–2020 in Lanzhou, the SSA seems to be positively correlated with aerosol absorption, while the AAE was determined by the relative contribution of EC and non-EC absorbing species (i.e., FS and OM).

4.2. Influence of aerosol absorption on radiative forcing efficiency

The aerosol radiative forcing efficiency ($\Delta F/\tau$) determines the absolute value of radiative forcing. The relationships between SSA and parameter b of radiative forcing efficiency were investigated (Fig. 10), and it was found that $\Delta F/\tau$ strongly depended on SSA while no significant relationship was found between $\Delta F/\tau$ and b. This indicates that the aerosol cooling efficiency is mainly determined by SSA and, to a lesser extent, by particle size during winter in Lanzhou. This phenomenon is clearly different from the results in Nanjing, where $\Delta F/\tau$ is less correlated with SSA and more dependent on b (Shen et al., 2018). Aerosol absorption exerts a critical influence on the aerosol radiative forcing efficiency; this issue that warrants further study.

4.3. Comparison of aerosol absorption among cities across the world

Aerosol absorption is important for aerosol radiative forcing. Two parameters, SSA and the absorption coefficient, were used to summarize the aerosol absorption in different regions of China and across the world in recent years (since 2015) (Fig. 11). The SSA was relatively high and the absorption coefficient was low for low PM levels during the winter of 2019–2020 in Lanzhou. However, the SSA decreased and the absorption coefficient increased from low to high PM level during the same period. The absorption coefficients of low and moderate PM levels were comparable to those of cities in other regions of China (Cheng et al., 2015; Deng et al., 2016; Wang et al., 2017a; Shen et al., 2018; Liao et al., 2020; Kong et al., 2020) and higher than those of European and American cities (Lim et al., 2018; Schmeisser et al., 2018; Donateo et al., 2020; Venter et al., 2020). The absorption coefficient at high PM level in Lanzhou was even higher than that of Delhi, Indian (Tiwari et al., 2015). Furthermore, the SSA in Lanzhou was much lower than that in Delhi, indicating strong aerosol absorption in Lanzhou. The sample number of the high PM level accounted half of the total samples.

Aerosol absorption coefficients are largely related to aerosol loadings, while SSAs are determined by the relative contributions of light scattering and absorption. In Sanya, a tourist city in China, both the absorption coefficient and the SSA are low (S1 in Fig. 11). The low

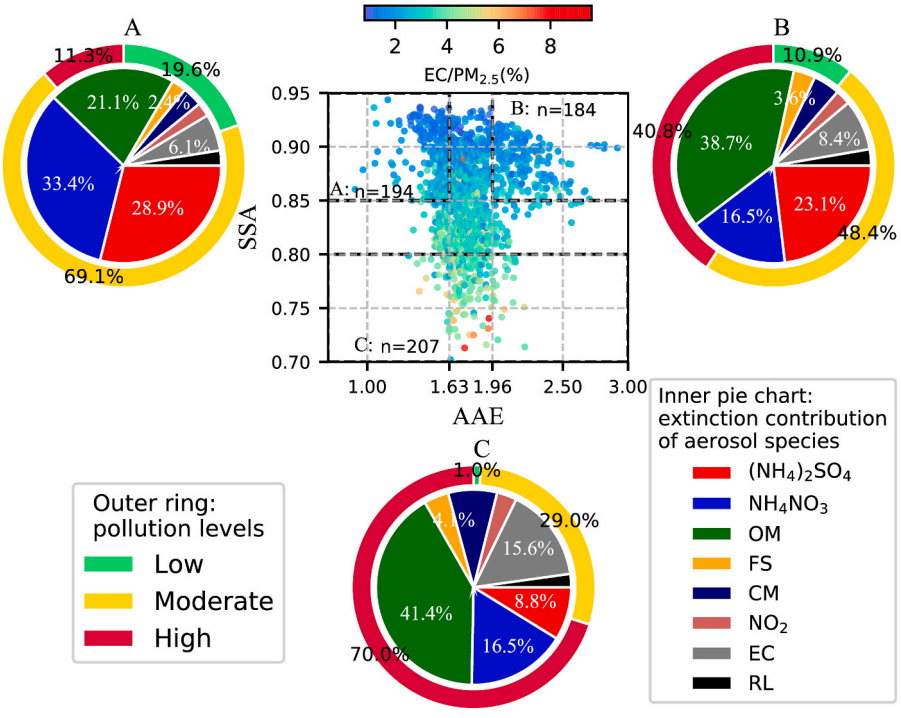

Fig. 9. Relationships among optical parameters (SSA and AAE), chemical compositions, and pollution levels.

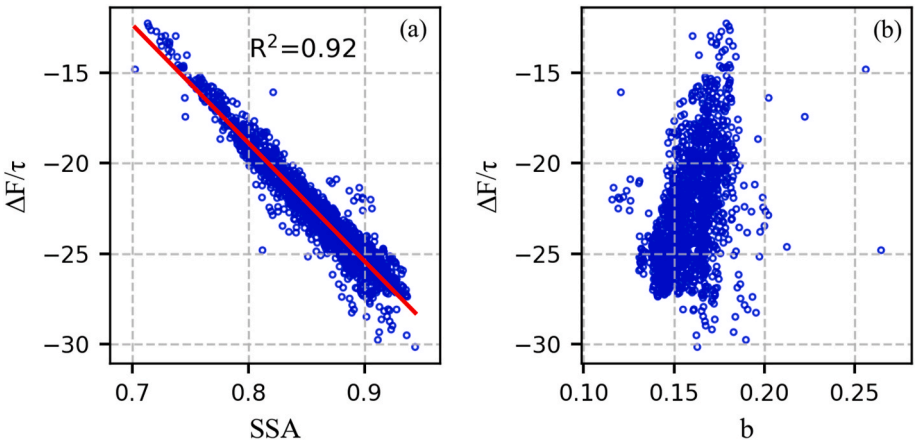

Fig. 10. Aerosol radiative forcing efficiency as a function of SSA (a) and b (b).

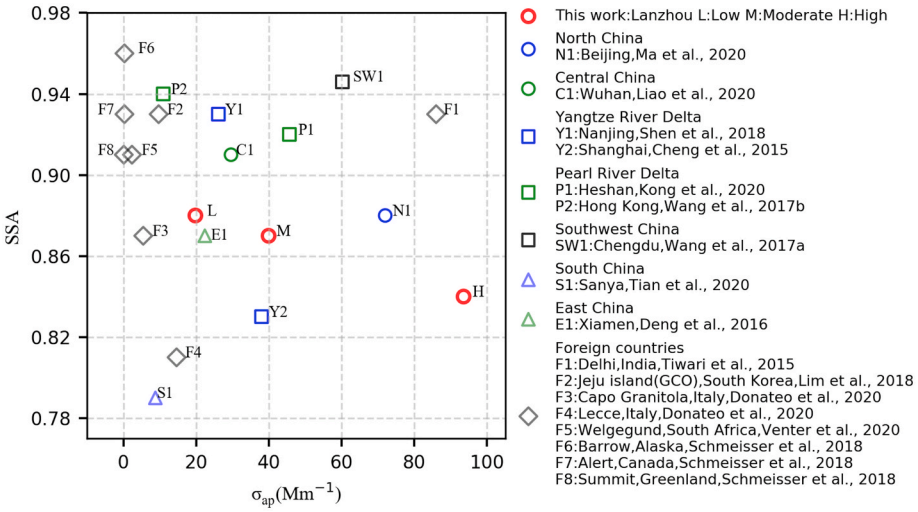

Fig. 11. Comparison of aerosol absorption in Lanzhou and other sites.

pollution level in Sanya results in a low absorption coefficient. The traffic emissions and biomass burning are the main sources of air pollution in Sanya in addition to the ocean emissions, which cause a relatively high contribution of EC (15%) and low contribution of SIAs (64%) to the aerosol extinction (Tian et al., 2020) compared to other cities. Thus, the SSA is also low in Sanya. In the suburbs of Hong Kong, the absorption coefficient is low and the SSA is high (P2 in Fig. 11). Similarly, the low absorption coefficient is related to low air pollution. However, the scattering aerosols (SIAs and OM) account for as much as 70.4% of the mass concentration of $PM_{2.5}$ in Hong Kong (Wang et al., 2018), which leads to strong scattering and relatively high SSAs. In Delhi, one of the most polluted cities in the world, both the absorption coefficient and SSA are high (F1 in Fig. 11). High air pollution leads to a high absorption coefficient and the average wintertime $PM_{2.5}$ concentration can reach 195.3 μg m^{-3} (Tiwari et al., 2015). Secondary aerosols are the most important sources of pollution (Sharma et al., 2017) and scattering aerosols (SIAs and OM) account for ~75% of the mass concentration of $PM_{2.5}$ (Tobler et al., 2020), which leads to high SSAs in Delhi. The absorption coefficient is high and SSA is low in the present study of Lanzhou for the high pollution level (H in Fig. 11), which may be explained by the relatively high contribution of EC and low contribution of SIAs to $PM_{2.5}$ under high pollution during winter (Section 3.2 and Du et al., 2020).

5. Summary and conclusions

To clarify the evolution of aerosol absorption and quantify the contribution of absorbing species under different severities of particulate pollution, aerosol absorption from low to high particulate pollution was investigated via intensive observations of aerosol optical properties during the winter of 2019–2020 in Lanzhou, Northwest China.

The scattering coefficient linearly increased with increasing $PM_{2.5}$ while the absorption coefficient increased more rapidly when $PM_{2.5}$ exceeded 69 μg m^{-3}, leading to a rapid decrease in the SSA and sharp increase in $MAE_{PM2.5}$ under high particulate pollution. Single scattering albedo ($MAE_{PM2.5}$) decreased (increased) from 0.87 (0.76) in the lowest $PM_{2.5}$ bin to 0.82 (1.11) in the highest $PM_{2.5}$ bin. Low humidity led to limited aerosol scattering enhancement and the linear relationship between the scattering coefficient and $PM_{2.5}$ was attributed to decreases in aerosol hygroscopicity with increasing $PM_{2.5}$.

Elemental carbon, FS, and OC accounted for 77.4%, 16.6%, and 6.0% of the total aerosol absorption, respectively. From low to high pollution levels, the contribution of EC absorption increased from 68.3% to 80.5% while that of FS decreased from 25.5% to 13.9%.

The calculated aerosol radiative forcing efficiency was strongly correlated with SSA, showing the importance of aerosol absorption for aerosol radiative forcing. Our results show the unique behavior of a rapid increase in aerosol absorption under high particulate pollution during winter in Lanzhou, which is opposite to the trends observed in

eastern Chinese cities, where SSA increases with increasing $PM_{2.5}$. However, the radiative forcing of light-absorbing materials (i.e., BC, mineral dust, and BrC) must be quantified in future studies.

CRediT authorship contribution statement

Xu Guan: Formal analysis, Data curation, Methodology, Software, Visualization, Writing - original draft, Writing - review & editing. **Min Wang:** Data curation, Formal analysis, Writing - original draft. **Tao Du:** Data curation, Software, Visualization. **Pengfei Tian:** Conceptualization, Formal analysis, Funding acquisition, Project administration, Validation, Writing - original draft, Writing - review & editing. **Naiyue Zhang:** Writing - review & editing. **Jinsen Shi:** Investigation. **Yi Chang:** Investigation. **Lei Zhang:** Funding acquisition, Resources, Supervision. **Min Zhang:** Visualization. **Xin Song:** Writing - review & editing. **Yijia Sun:** Writing - review & editing.

Declaration of competing interest

The authors declare that they have no known competing financial interests or personal relationships that could have appeared to influence the work reported in this paper.

Acknowledgement and data availability

This research was supported by the National Natural Science Foundation of China (41905017), the Foundation for Innovative Research Groups of the National Natural Science Foundation of China (41521004), and the Fundamental Research Funds for the Central Universities (lzujbky-2020-36 and lzujbky-2020-kb31). The authors thank the staffs from the Lanzhou Atmospheric Components Monitoring Superstation (LACMS) for the aerosol optical and supporting data. The LACMS data is available online at the Semi-Arid Climate and Environment Observatory of Lanzhou University (SACOL, http://climate.lzu.edu.cn/English/Data_Sharing/LACMS_data.htm).

Appendix A. Supplementary data

Supplementary data to this article can be found online at https://doi.org/10.1016/j.atmosenv.2020.118081.

References

Allen, R.J., Sherwood, S.C., Norris, J.R., Zender, C.S., 2012. Recent Northern Hemisphere tropical expansion primarily driven by black carbon and tropospheric ozone. Nature 485, 350–354. https://doi.org/10.1038/nature11097.

Andreae, M.O., Gelencsér, A., 2006. Black carbon or brown carbon? The nature of light-absorbing carbonaceous aerosols. Atmos. Chem. Phys. 6, 3131–3148. https://doi.org/10.5194/acp-6-3131-2006.

Barman, N., Roy, R., Saha, B., Kundu, S.S., Borgohain, A., De, B.K., Guha, A., 2019. Investigation of seasonal variation of compensation parameter and absorption Ångström Exponent of aerosol after loading correction over a remote station in north-east India. Atmos. Environ. 212, 106–115. https://doi.org/10.1016/j.atmosenv.2019.05.036.

Bellouin, N., Quaas, J., Gryspeerdt, E., Kinne, S., Stier, P., Watson-Parris, D., Boucher, O., Carslaw, K.S., Christensen, M., Daniau, A.L., Dufresne, J.L., Feingold, G., Fiedler, S., Forster, P., Gettelman, A., Haywood, J.M., Lohmann, U., Malavelle, F., Mauritsen, T., McCoy, D.T., Myhre, G., Mülmenstädt, J., Neubauer, D., Possner, A., Rugenstein, M., Sato, Y., Schulz, M., Schwartz, S.E., Sourdeval, O., Storelvmo, T., Toll, V., Winker, D., Stevens, B., 2020. Bounding global aerosol radiative forcing of climate change. Rev. Geophys. 58, e2019RG000660 https://doi.org/10.1029/2019RG000660.

Bergin, M.H., Tripathi, S.N., Jai Devi, J., Gupta, T., McKenzie, M., Rana, K.S., Shafer, M. M., Villalobos, A.M., Schauer, J.J., 2015. The discoloration of the taj mahal due to particulate carbon and dust deposition. Environ. Sci. Technol. 49, 808–812. https://doi.org/10.1021/es504005q.

Bond, T.C., Bergstrom, R.W., 2006. Light absorption by carbonaceous particles: an investigative review. Aerosol. Sci. Technol. 40, 27–67. https://doi.org/10.1080/02786820500421521.

Bond, T.C., Doherty, S.J., Fahey, D.W., Forster, P.M., Berntsen, T., DeAngelo, B.J., Flanner, M.G., Ghan, S., Kärcher, B., Koch, D., Kinne, S., Kondo, Y., Quinn, P.K., Sarofim, M.C., Schultz, M.G., Schulz, M., Venkataraman, C., Zhang, H., Zhang, S., Bellouin, N., Guttikunda, S.K., Hopke, P.K., Jacobson, M.Z., Kaiser, J.W., Klimont, Z., Lohmann, U., Schwarz, J.P., Shindell, D., Storelvmo, T., Warren, S.G., Zender, C.S., 2013. Bounding the role of black carbon in the climate system: a scientific assessment. J. Geophys. Res.: Atmosphere 118, 5380–5552. https://doi.org/10.1002/jgrd.50171.

Bond, T.C., Habib, G., Bergstrom, R.W., 2006. Limitations in the enhancement of visible light absorption due to mixing state. J. Geophys. Res.: Atmosphere 111. https://doi.org/10.1029/2006JD007315.

Brink, H., Otjes, R., Weijers, E., 2019. Extreme levels and chemistry of PM from the consumer fireworks in The Netherlands. Atmos. Environ. 212, 36–40. https://doi.org/10.1016/j.atmosenv.2019.04.046.

Cao, J., Wang, Q., Chow, J.C., Watson, J.G., Tie, X., Shen, Z., Wang, P., An, Z., 2012. Impacts of aerosol compositions on visibility impairment in Xi'an, China. Atmos. Environ. 59, 559–566. https://doi.org/10.1016/j.atmosenv.2012.05.036.

Cappa, C.D., Onasch, T.B., Massoli, P., Worsnop, D.R., Bates, T.S., Cross, E.S., Davidovits, P., Hakala, J., Hayden, K.L., Jobson, B.T., Kolesar, K.R., Lack, D.A., Lerner, B.M., Li, S.-M., Mellon, D., Nuaaman, I., Olfert, J.S., Petäjä, T., Quinn, P.K., Song, C., Subramanian, R., Williams, E.J., Zaveri, R.A., 2012. Radiative absorption enhancements due to the mixing state of atmospheric black carbon. Science 337, 1078. https://doi.org/10.1126/science.1223447.

Carrico, C.M., Kus, P., Rood, M.J., Quinn, P.K., Bates, T.S., 2003. Mixtures of pollution, dust, sea salt, and volcanic aerosol during ACE-Asia: radiative properties as a function of relative humidity. J. Geophys. Res.: Atmosphere 108. https://doi.org/10.1029/2003JD003405.

Chan, Y.C., Simpson, R.W., McTainsh, G.H., Vowles, P.D., Cohen, D.D., Bailey, G.M., 1999. Source apportionment of visibility degradation problems in Brisbane (Australia) using the multiple linear regression techniques. Atmos. Environ. 33, 3237–3250. https://doi.org/10.1016/S1352-2310(99)00091-6.

Cheng, Y., He, K.B., Zheng, M., Duan, F.K., Du, Z.Y., Ma, Y.L., Tan, J.H., Yang, F.M., Liu, J.M., Zhang, X.L., Weber, R.J., Bergin, M.H., Russell, A.G., 2011. Mass absorption efficiency of elemental carbon and water-soluble organic carbon in Beijing, China. Atmos. Chem. Phys. 11, 11497–11510. https://doi.org/10.5194/acp-11-11497-2011.

Cheng, Z., Jiang, J., Chen, C., Gao, J., Wang, S., Watson, J.G., Wang, H., Deng, J., Wang, B., Zhou, M., Chow, J.C., Pitchford, M.L., Hao, J., 2015. Estimation of aerosol mass scattering efficiencies under high mass loading: case study for the megacity of Shanghai, China. Environ. Sci. Technol. 49, 831–838. https://doi.org/10.1021/es504567q.

Cheng, Z., Wang, S., Qiao, L., Wang, H., Zhou, M., Fu, X., Lou, S., Luo, L., Jiang, J., Chen, C., Wang, X., Hao, J., 2018. Insights into extinction evolution during extreme low visibility events: case study of Shanghai, China. Sci. Total Environ. 618, 793–803. https://doi.org/10.1016/j.scitotenv.2017.08.202.

Chin, M., Diehl, T., Dubovik, O., Eck, T.F., Holben, B.N., Sinyuk, A., Streets, D.G., 2009. Light absorption by pollution, dust, and biomass burning aerosols: a global model study and evaluation with AERONET measurements. Ann. Geophys. 27, 3439–3464. https://doi.org/10.5194/angeo-27-3439-2009.

Cho, C., Kim, S.-W., Lee, M., Lim, S., Fang, W., Gustafsson, Ö., Andersson, A., Park, R.J., Sheridan, P.J., 2019. Observation-based estimates of the mass absorption cross-section of black and brown carbon and their contribution to aerosol light absorption in East Asia. Atmos. Environ. 212, 65–74. https://doi.org/10.1016/j.atmosenv.2019.05.024.

Chow, J.C., Watson, J.G., Chen, L.W.A., Arnott, W.P., Moosmüller, H., Fung, K., 2004. Equivalence of elemental carbon by thermal/optical reflectance and transmittance with different temperature protocols. Environ. Sci. Technol. 38, 4414–4422. https://doi.org/10.1021/es034936u.

Delene, D.J., Ogren, J.A., 2002. Variability of aerosol optical properties at four north American surface monitoring sites. J. Atmos. Sci. 59, 1135–1150. https://doi.org/10.1175/1520-0469(2002)059%3C1135:VOAOPA%3E2.0.CO;2.

Deng, J., Zhang, Y., Hong, Y., Xu, L., Chen, Y., Du, W., Chen, J., 2016. Optical properties of PM2.5 and the impacts of chemical compositions in the coastal city Xiamen in China. Sci. Total Environ. 557–558, 665–675. https://doi.org/10.1016/j.scitotenv.2016.03.143.

Devi, J.J., Bergin, M.H., McKenzie, M., Schauer, J.J., Weber, R.J., 2016. Contribution of particulate brown carbon to light absorption in the rural and urban Southeast US. Atmos. Environ. 136, 95–104. https://doi.org/10.1016/j.atmosenv.2016.04.011.

Ding, A.J., Huang, X., Nie, W., Sun, J.N., Kerminen, V.M., Petäjä, T., Su, H., Cheng, Y.F., Yang, X.Q., Wang, M.H., Chi, X.G., Wang, J.P., Virkkula, A., Guo, W.D., Yuan, J., Wang, S.Y., Zhang, R.J., Wu, Y.F., Song, Y., Zhu, T., Zilitinkevich, S., Kulmala, M., Fu, C.B., 2016. Enhanced haze pollution by black carbon in megacities in China. Geophys. Res. Lett. 43, 2873–2879. https://doi.org/10.1002/2016GL067745.

Donateo, A., Lo Feudo, T., Marinoni, A., Calidonna, C.R., Contini, D., Bonasoni, P., 2020. Long-term observations of aerosol optical properties at three GAW regional sites in the Central Mediterranean. Atmos. Res. 241, 104976. https://doi.org/10.1016/j.atmosres.2020.104976.

Du, T., Wang, M., Guan, X., Zhang, M., Zeng, H., Chang, Y., Zhang, L., Tian, P., Shi, J., Tang, C., 2020. Characteristics and formation mechanisms of winter particulate pollution in Lanzhou, northwest China. J. Geophys. Res.: Atmosphere 125, e2020JD033369. https://doi.org/10.1029/2020JD033369.

Fan, J., Rosenfeld, D., Yang, Y., Zhao, C., Leung, L.R., Li, Z., 2015. Substantial contribution of anthropogenic air pollution to catastrophic floods in Southwest China. Geophys. Res. Lett. 42, 6066–6075. https://doi.org/10.1002/2015GL064479.

Feng, Y., Ramanathan, V., Kotamarthi, V.R., 2013. Brown carbon: a significant atmospheric absorber of solar radiation? Atmos. Chem. Phys. 13, 8607–8621. https://doi.org/10.5194/acp-13-8607-2013.

Ferrero, L., Močnik, G., Cogliati, S., Gregorič, A., Colombo, R., Bolzacchini, E., 2018. Heating rate of light absorbing aerosols: time-resolved measurements, the role of

clouds, and source identification. Environ. Sci. Technol. 52, 3546–3555. https://pubs.acs.org/doi/abs/10.1021/acs.est.7b04320.
Han, T., Qiao, L., Zhou, M., Qu, Y., Du, J., Liu, X., Lou, S., Chen, C., Wang, H., Zhang, F., Yu, Q., Wu, Q., 2015. Chemical and optical properties of aerosols and their interrelationship in winter in the megacity Shanghai of China. J. Environ. Sci. 27, 59–69. https://doi.org/10.1016/j.jes.2014.04.018.
Hassan, T., Moosmüller, H., Chung, C.E., 2015. Coefficients of an analytical aerosol forcing equation determined with a Monte-Carlo radiation model. J. Quant. Spectrosc. Radiat. Transf. 164, 129–136. https://doi.org/10.1016/j.jqsrt.2015.05.015.
Haywood, J., Ramaswamy, V., 1998. Global sensitivity studies of the direct radiative forcing due to anthropogenic sulfate and black carbon aerosols. J. Geophys. Res. 103, 6043–6058. https://doi.org/10.1029/97JD03426.
Haywood, J.M., Shine, K.P., 1995. The effect of anthropogenic sulfate and soot aerosol on the clear sky planetary radiation budget. Geophys. Res. Lett. 22, 603–606. https://doi.org/10.1029/95GL00075.
Hodkinson, J.R., 1966. Calculation of colour and visibility in urban atmospheres polluted by gaseous NO2. Air Water Pollut. 10, 137–144.
Hu, Z., Huang, J., Zhao, C., Bi, J., Jin, Q., Qian, Y., Leung, L.R., Feng, T., Chen, S., Ma, J., 2019. Modeling the contributions of Northern Hemisphere dust sources to dust outflow from East Asia. Atmos. Environ. 202, 234–243. https://doi.org/10.1016/j.atmosenv.2019.01.022.
IPCC, 2013. Climate Change 2013: the Physical Science Basis. Contribution of Working Group I to the Fifth Assessment Report of the Intergovernmental Panel on Climate Change. Cambridge University Press, Cambridge, United Kingdom and New York, NY, USA.
Jacobson, M.Z., 2001. Strong radiative heating due to the mixing state of black carbon in atmospheric aerosols. Nature 409, 695–697. https://doi.org/10.1038/35055518.
Janssen, N.A.H., Hoek, G., Simic-Lawson, M., Fischer, P., van Bree, L., ten Brink, H., Keuken, M., Atkinson, R.W., Anderson, H.R., Brunekreef, B., Cassee, F.R., 2011. Black carbon as an additional indicator of the adverse health effects of airborne particles compared with PM10 and PM2.5. Environ. Health Perspect. 119, 1691–1699. https://doi.org/10.1289/ehp.1003369.
Kang, L., Chen, S., Huang, J., Zhao, S., Ma, X., Yuan, T., Zhang, X., Xie, T., 2017. The spatial and temporal distributions of absorbing aerosols over east asia. Rem. Sens. 9 https://doi.org/10.3390/rs9101050.
Kong, L., Hu, M., Tan, Q., Feng, M., Qu, Y., An, J., Zhang, Y., Liu, X., Cheng, N., 2020. Aerosol optical properties under different pollution levels in the Pearl River Delta (PRD) region of China. J. Environ. Sci. 87, 49–59. https://doi.org/10.1016/j.jes.2019.02.019.
Koschmieder, H., 1924. Theorie der horizontalen Sichtweite. Keim & Nemnich.
Lack, D.A., Cappa, C.D., 2010. Impact of brown and clear carbon on light absorption enhancement, single scatter albedo and absorption wavelength dependence of black carbon. Atmos. Chem. Phys. 10, 4207–4220. https://doi.org/10.5194/acp-10-4207-2010.
Lack, D.A., Langridge, J.M., 2013. On the attribution of black and brown carbon light absorption using the Ångström exponent. Atmos. Chem. Phys. 13, 10535–10543. https://doi.org/10.5194/acp-13-10535-2013.
Liao, W., Zhou, J., Zhu, S., Xiao, A., Li, K., Schauer, J.J., 2020. Characterization of aerosol chemical composition and the reconstruction of light extinction coefficients during winter in Wuhan, China. Chemosphere 241, 125033. https://doi.org/10.1016/j.chemosphere.2019.125033.
Lim, S., Lee, M., Kim, S.-W., Laj, P., 2018. Sulfate alters aerosol absorption properties in East Asian outflow. Sci. Rep. 8, 5172. https://doi.org/10.1038/s41598-018-23021-1.
Liu, D., Hu, K., Zhao, D., Ding, S., Wu, Y., Zhou, C., Yu, C., Tian, P., Liu, Q., Bi, K., Wu, Y., Hu, B., Ji, D., Kong, S., Ouyang, B., He, H., Huang, M., Ding, D., 2020. Efficient vertical transport of black carbon in the planetary boundary layer. Geophys. Res. Lett. 47 https://doi.org/10.1029/2020GL088858.
Liu, D., Whitehead, J., Alfarra, M.R., Reyes-Villegas, E., Spracklen, Dominick V., Reddington, Carly L., Kong, S., Williams, Paul I., Ting, Y.-C., Haslett, S., Taylor, Jonathan W., Flynn, Michael J., Morgan, William T., McFiggans, G., Coe, H., Allan, James D., 2017. Black-carbon absorption enhancement in the atmosphere determined by particle mixing state. Nat. Geosci. 10, 184–188. https://doi.org/10.1038/ngeo2901.
Liu, X., Cheng, Y., Zhang, Y., Jung, J., Sugimoto, N., Chang, S.-Y., Kim, Y.J., Fan, S., Zeng, L., 2008. Influences of relative humidity and particle chemical composition on aerosol scattering properties during the 2006 PRD campaign. Atmos. Environ. 42, 1525–1536. https://doi.org/10.1016/j.atmosenv.2007.10.077.
Ma, Q., Wu, Y., Fu, S., Zhang, D., Han, Z., Zhang, R., 2020. Pollution severity-dependent aerosol light scattering enhanced by inorganic species formation in Beijing haze. Sci. Total Environ. 719, 137545. https://doi.org/10.1016/j.scitotenv.2020.137545.
Marshall, S.F., Covert, D.S., Charlson, R.J., 1995. Relationship between asymmetry parameter and hemispheric backscatter ratio: implications for climate forcing by aerosols. Appl. Optic. 34, 6306–6311. https://doi.org/10.1364/AO.34.006306.
Miller, R.L., Tegen, I., 1998. Climate response to soil dust aerosols. J. Clim. 11, 3247–3267. https://doi.org/10.1175/1520-0442(1998)011%3C3247:CRTSDA%3E2.0.CO;2.
Myhre, G., Samset, B.H., Schulz, M., Balkanski, Y., Bauer, S., Berntsen, T.K., Bian, H., Bellouin, N., Chin, M., Diehl, T., Easter, R.C., Feichter, J., Ghan, S.J., Hauglustaine, D., Iversen, T., Kinne, S., Kirkevåg, A., Lamarque, J.F., Lin, G., Liu, X., Lund, M.T., Luo, G., Ma, X., van Noije, T., Penner, J.E., Rasch, P.J., Ruiz, A., Seland, Ø., Skeie, R.B., Stier, P., Takemura, T., Tsigaridis, K., Wang, P., Wang, Z., Xu, L., Yu, H., Yu, F., Yoon, J.H., Zhang, K., Zhang, H., Zhou, C., 2013. Radiative forcing of the direct aerosol effect from AeroCom Phase II simulations. Atmos. Chem. Phys. 13, 1853–1877. https://doi.org/10.5194/acp-13-1853-2013.
Peng, J., Hu, M., Guo, S., Du, Z., Zheng, J., Shang, D., Levy Zamora, M., Zeng, L., Shao, M., Wu, Y.-S., Zheng, J., Wang, Y., Glen, C.R., Collins, D.R., Molina, M.J., Zhang, R., 2016. Markedly enhanced absorption and direct radiative forcing of black carbon under polluted urban environments. Proc. Natl. Acad. Sci. U. S. A. 113, 4266–4271. https://doi.org/10.1073/pnas.1602310113.
Petzold, A., Ogren, J.A., Fiebig, M., Laj, P., Li, S.M., Baltensperger, U., Holzer-Popp, T., Kinne, S., Pappalardo, G., Sugimoto, N., Wehrli, C., Wiedensohler, A., Zhang, X.Y., 2013. Recommendations for reporting "black carbon" measurements. Atmos. Chem. Phys. 13, 8365–8379. https://doi.org/10.5194/acp-13-8365-2013.
Pitchford, M., Malm, W., Schichtel, B., Kumar, N., Lowenthal, D., Hand, J., 2007. Revised algorithm for estimating light extinction from IMPROVE particle speciation data. J. Air Waste Manag. Assoc. 57, 1326–1336. https://doi.org/10.3155/1047-3289.57.11.1326.
Ramanathan, V., Carmichael, G., 2008. Global and regional climate changes due to black carbon. Nat. Geosci. 1, 221–227. https://doi.org/10.1038/ngeo156.
Sato, M., Hansen, J., Koch, D., Lacis, A., Ruedy, R., Dubovik, O., Holben, B., Chin, M., Novakov, T., 2003. Global atmospheric black carbon inferred from AERONET. Proc. Natl. Acad. Sci. Unit. States Am. 100, 6319. https://doi.org/10.1073/pnas.0731897100.
Schmeisser, L., Backman, J., Ogren, J.A., Andrews, E., Asmi, E., Starkweather, S., Uttal, T., Fiebig, M., Sharma, S., Eleftheriadis, K., Vratolis, S., Bergin, M., Tunved, P., Jefferson, A., 2018. Seasonality of aerosol optical properties in the Arctic. Atmos. Chem. Phys. 18, 11599–11622. https://doi.org/10.5194/acp-18-11599-2018.
Segura, S., Estellés, V., Esteve, A.R., Marcos, C.R., Utrillas, M.P., Martínez-Lozano, J.A., 2016. Multiyear in-situ measurements of atmospheric aerosol absorption properties at an urban coastal site in western Mediterranean. Atmos. Environ. 129, 18–26. https://doi.org/10.1016/j.atmosenv.2016.01.008.
Sharma, S.K., Mandal, T.K., 2017. Chemical composition of fine mode particulate matter (PM2.5) in an urban area of Delhi, India and its source apportionment. Urban Climate 21, 106–122. https://doi.org/10.1016/j.uclim.2017.05.009.
Shen, Y., Virkkula, A., Ding, A., Wang, J., Chi, X., Nie, W., Qi, X., Huang, X., Liu, Q., Zheng, L., Xu, Z., Petäjä, T., Aalto, P.P., Fu, C., Kulmala, M., 2018. Aerosol optical properties at SORPES in Nanjing, east China. Atmos. Chem. Phys. 18, 5265–5292. https://doi.org/10.5194/acp-18-5265-2018.
Sheridan, P.J., Ogren, J.A., 1999. Observations of the vertical and regional variability of aerosol optical properties over central and eastern North America. J. Geophys. Res.: Atmosphere 104, 16793–16805. https://doi.org/10.1029/1999JD900241.
Shindell, D., Kuylenstierna, J.C.I., Vignati, E., van Dingenen, R., Amann, M., Klimont, Z., Anenberg, S.C., Muller, N., Janssens-Maenhout, G., Raes, F., Schwartz, J., Faluvegi, G., Pozzoli, L., Kupiainen, K., Höglund-Isaksson, L., Emberson, L., Streets, D., Ramanathan, V., Hicks, K., Oanh, N.T.K., Milly, G., Williams, M., Demkine, V., Fowler, D., 2012. Simultaneously mitigating near-term climate change and improving human health and food security. Science 335, 183. https://doi.org/10.1126/science.1210026.
Svenningsson, I.B., Hansson, H.C., Wiedensohler, A., Ogren, J.A., Noone, K.J., Hallberg, A., 1992. Hygroscopic growth of aerosol particles in the Po Valley. Tellus B 44, 556–569. https://doi.org/10.1034/j.1600-0889.1992.t01-1-00009.x.
Tan, J., Zhang, L., Zhou, X., Duan, J., Li, Y., Hu, J., He, K., 2017. Chemical characteristics and source apportionment of PM2.5 in Lanzhou, China. Sci. Total Environ. 601–602, 1743–1752. https://doi.org/10.1016/j.scitotenv.2017.06.050.
Tao, J., Zhang, L., Gao, J., Wang, H., Chai, F., Wang, S., 2015. Aerosol chemical composition and light scattering during a winter season in Beijing. Atmos. Environ. 110, 36–44. https://doi.org/10.1016/j.atmosenv.2015.03.037.
Tao, J., Zhang, L., Ho, K., Zhang, R., Lin, Z., Zhang, Z., Lin, M., Cao, J., Liu, S., Wang, G., 2014. Impact of PM2.5 chemical compositions on aerosol light scattering in Guangzhou — the largest megacity in South China. Atmos. Res. 135–136, 48–58. https://doi.org/10.1016/j.atmosres.2013.08.015.
Tao, M., Wang, L., Chen, L., Wang, Z., Tao, J., 2020. Reversal of aerosol properties in eastern China with rapid decline of anthropogenic emissions. Rem. Sens. 12, 523. https://doi.org/10.3390/rs12030523.
Tian, J., Wang, Q., Han, Y., Ye, J., Wang, P., Pongpiachan, S., Ni, H., Zhou, Y., Wang, M., Zhao, Y., Cao, J., 2020. Contributions of aerosol composition and sources to particulate optical properties in a southern coastal city of China. Atmos. Res. 235, 104744. https://doi.org/10.1016/j.atmosres.2019.104744.
Tian, M., Wang, H., Chen, Y., Yang, F., Zhang, X., Zou, Q., Zhang, R., Ma, Y., He, K., 2016. Characteristics of aerosol pollution during heavy haze events in Suzhou, China. Atmos. Chem. Phys. 16, 7357–7371. https://doi.org/10.5194/acp-16-7357-2016.
Tian, P., Cao, X., Zhang, L., Wang, H., Shi, J., Huang, Z., Zhou, T., Liu, H., 2015. Observation and simulation study of atmospheric aerosol nonsphericity over the Loess Plateau in northwest China. Atmos. Environ. 117, 212–219. https://doi.org/10.1016/j.atmosenv.2015.07.020.
Tian, P., Zhang, L., Ma, J., Tang, K., Xu, L., Wang, Y., Cao, X., Liang, J., Ji, Y., Jiang, J.H., Yung, Y.L., Zhang, R., 2018. Radiative absorption enhancement of dust mixed with anthropogenic pollution over East Asia. Atmos. Chem. Phys. 18, 7815–7825. https://doi.org/10.5194/acp-18-7815-2018.
Titos, G., Alados-Arboledas, L., Granados-Munoz, M.J., Andrews, E., Cazorla, A., 2016. Effect of hygroscopic growth on the aerosol light-scattering coefficient: a review of measurements, techniques and error sources. Atmos. Environ. 141, 494–507. https://doi.org/10.1016/j.atmosenv.2016.07.021.
Tiwari, S., Pandithurai, G., Attri, S.D., Srivastava, A.K., Soni, V.K., Bisht, D.S., Anil Kumar, V., Srivastava, M.K., 2015. Aerosol optical properties and their relationship with meteorological parameters during wintertime in Delhi, India. Atmos. Res. 153, 465–479. https://doi.org/10.1016/j.atmosres.2014.10.003.
Tobler, A., Bhattu, D., Canonaco, F., Lalchandani, V., Shukla, A., Thamban, N.M., Mishra, S., Srivastava, A.K., Bisht, D.S., Tiwari, S., Singh, S., Močnik, G.,

Baltensperger, U., Tripathi, S.N., Slowik, J.G., Prévôt, A.S.H., 2020. Chemical characterization of PM2.5 and source apportionment of organic aerosol in New Delhi, India. Sci. Total Environ. 745, 140924. https://doi.org/10.1016/j.scitotenv.2020.140924.

Twomey, S., 1977. The influence of pollution on the shortwave albedo of clouds. Journal of The Atmospheric Sciences - J ATMOS SCI 34, 1149–1154. https://doi.org/10.1175/1520-0469(1977)034%3C1149:TIOPOT%3E2.0.CO;2.

Valenzuela, A., Olmo, F.J., Lyamani, H., Antón, M., Titos, G., Cazorla, A., Alados-Arboledas, L., 2015. Aerosol scattering and absorption Angström exponents as indicators of dust and dust-free days over Granada (Spain). Atmos. Res. 154, 1–13. https://doi.org/10.1016/j.atmosres.2014.10.015.

Venter, M., Beukes, J.P., Gideon van Zyl, P., Vakkari, V., Virkkula, A., Josipovic, M., Kulmala, M., Laakso, L., 2020. Six-year observations of aerosol optical properties at a southern African grassland savannah site. Atmos. Environ. 230, 117477. https://doi.org/10.1016/j.atmosenv.2020.117477.

Virkkula, A., Backman, J., Aalto, P.P., Hulkkonen, M., Riuttanen, L., Nieminen, T., dal Maso, M., Sogacheva, L., de Leeuw, G., Kulmala, M., 2011. Seasonal cycle, size dependencies, and source analyses of aerosol optical properties at the SMEAR II measurement station in Hyytiälä, Finland. Atmos. Chem. Phys. 11, 4445–4468. https://doi.org/10.5194/acp-11-4445-2011.

Wang, G., Zhang, R., Gomez, M.E., Yang, L., Levy Zamora, M., Hu, M., Lin, Y., Peng, J., Guo, S., Meng, J., Li, J., Cheng, C., Hu, T., Ren, Y., Wang, Y., Gao, J., Cao, J., An, Z., Zhou, W., Li, G., Wang, J., Tian, P., Marrero-Ortiz, W., Secrest, J., Du, Z., Zheng, J., Shang, D., Zeng, L., Shao, M., Wang, W., Huang, Y., Wang, Y., Zhu, Y., Li, Y., Hu, J., Pan, B., Cai, L., Cheng, Y., Ji, Y., Zhang, F., Rosenfeld, D., Liss, P.S., Duce, R.A., Kolb, C.E., Molina, M.J., 2016. Persistent sulfate formation from London Fog to Chinese haze. Proc. Natl. Acad. Sci. Unit. States Am. 113, 13630. https://doi.org/10.1073/pnas.1616540113.

Wang, H., Shi, G., Tian, M., Zhang, L., Chen, Y., Yang, F., Cao, X., 2017a. Aerosol optical properties and chemical composition apportionment in Sichuan Basin, China. Sci. Total Environ. 577, 245–257. https://doi.org/10.1016/j.scitotenv.2016.10.173.

Wang, J., Virkkula, A., Gao, Y., Lee, S., Shen, Y., Chi, X., Nie, W., Liu, Q., Xu, Z., Huang, X., Wang, T., Cui, L., Ding, A., 2017b. Observations of aerosol optical properties at a coastal site in Hong Kong, South China. Atmos. Chem. Phys. 17, 2653–2671. https://doi.org/10.5194/acp-17-2653-2017.

Wang, T., Du, Z., Tan, T., Xu, N., Hu, M., Hu, J., Guo, S., 2019. Measurement of aerosol optical properties and their potential source origin in urban Beijing from 2013-2017. Atmos. Environ. 206, 293–302. https://doi.org/10.1016/j.atmosenv.2019.02.049.

Wang, Y., Wu, Z., Ma, N., Wu, Y., Zeng, L., Zhao, C., Wiedensohler, A., 2018. Statistical analysis and parameterization of the hygroscopic growth of the sub-micrometer urban background aerosol in Beijing. Atmos. Environ. 175, 184–191. https://doi.org/10.1016/j.atmosenv.2017.12.003.

Weinzierl, B, Sauer, D, Esselborn, M, Petzold, A, Lambert, A, Rose, M, Mund, S, Wirth, M, Ansmann, A, Tesche, M, Gross, S, 2011. Microphysical and optical properties of dust and tropical biomass burning aerosol layers in the Cape Verde region – An overview of the airborne in situ and lidar measurements during SAMUM-2. Tellus B 63, 589–618. https://doi.org/10.1111/j.1600-0889.2011.00566.x.

Xu, J., Shi, J., Zhang, Q., Wang, J., Canonaco, F., Prevot, A., Vonwiller, M., Szidat, S., Ge, J., Ma, J., An, Y., Kang, S., Qin, D., 2016. Wintertime organic and inorganic aerosols in Lanzhou, China: sources, processes and comparison with the results during summer. Atmos. Chem. Phys. Discuss. 1–52. https://doi.org/10.5194/acp-16-14937-2016.

Yang, M., Howell, S.G., Zhuang, J., Huebert, B.J., 2009. Attribution of aerosol light absorption to black carbon, brown carbon, and dust in China – interpretations of atmospheric measurements during EAST-AIRE. Atmos. Chem. Phys. 9, 2035–2050. https://doi.org/10.5194/acp-9-2035-2009.

Yang, Y.R., Liu, X.G., Qu, Y., An, J.L., Jiang, R., Zhang, Y.H., Sun, Y.L., Wu, Z.J., Zhang, F., Xu, W.Q., Ma, Q.X., 2015. Characteristics and formation mechanism of continuous hazes in China: a case study during the autumn of 2014 in the North China Plain. Atmos. Chem. Phys. 15, 8165–8178. https://doi.org/10.5194/acp-15-8165-2015.

Yu, H., Kaufman, Y.J., Chin, M., Feingold, G., Remer, L.A., Anderson, T.L., Balkanski, Y., Bellouin, N., Boucher, O., Christopher, S., DeCola, P., Kahn, R., Koch, D., Loeb, N., Reddy, M.S., Schulz, M., Takemura, T., Zhou, M., 2006. A review of measurement-based assessments of the aerosol direct radiative effect and forcing. Atmos. Chem. Phys. 6, 613–666. https://doi.org/10.5194/acp-6-613-2006.

Zhang, F., Wang, Y., Peng, J., Chen, L., Sun, Y., Duan, L., Ge, X., Li, Y., Zhao, J., Liu, C., Zhang, X., Zhang, G., Pan, Y., Wang, Y., Zhang, A.L., Ji, Y., Wang, G., Hu, M., Molina, M.J., Zhang, R., 2020a. An unexpected catalyst dominates formation and radiative forcing of regional haze. Proc. Natl. Acad. Sci. Unit. States Am. 117, 3960. https://doi.org/10.1073/pnas.1919343117.

Zhang, X., Zhang, Y., Sun, J., Zheng, X., Li, G., Deng, Z., 2017. Characterization of particle number size distribution and new particle formation in an urban environment in Lanzhou, China. J. Aerosol Sci. 103, 53–66. https://doi.org/10.1016/j.jaerosci.2016.10.010.

Zhang, Y., Kang, S., 2019. Characteristics of carbonaceous aerosols analyzed using a multiwavelength thermal/optical carbon analyzer: a case study in Lanzhou City. Sci. China Earth Sci. 62, 389–402. https://doi.org/10.1007/s11430-017-9245-9.

Zhang, Y., Zhi, G., Jin, W., Wang, L., Guo, S., Shi, R., Sun, J., Cheng, M., Bi, F., Gao, J., Zhang, B., Wu, J., Shi, Z., Liu, B., Wang, Z., Li, S., 2020b. Differing effects of escalating pollution on absorption and scattering efficiencies of aerosols: toward co-beneficial air quality enhancement and climate protection measures. Atmos. Environ. 232, 117570. https://doi.org/10.1016/j.atmosenv.2020.117570.

Zhao, C., Yu, Y., Kuang, Y., Tao, J., Zhao, G., 2019. Recent progress of aerosol light-scattering enhancement factor studies in China. Adv. Atmos. Sci. 36, 1015–1026. https://doi.org/10.1007/s00376-019-8248-1.

Zhi, G., Chen, Y., Sun, J., Chen, L., Tian, W., Duan, J., Zhang, G., Chai, F., Sheng, G., Fu, J., 2011. Harmonizing aerosol carbon measurements between two conventional thermal/optical analysis methods. Environ. Sci. Technol. 45, 2902–2908. https://doi.org/10.1021/es102803f.

Zhou, Y., Wang, Q., Huang, R., Liu, S., Tie, X., Su, X., Niu, X., Zhao, Z., Ni, H., Wang, M., Zhang, Y., Cao, J., 2017. Optical properties of aerosols and implications for radiative effects in beijing during the asia-pacific economic cooperation summit 2014. J. Geophys. Res.: Atmosphere 122 (10), 119–132. https://doi.org/10.1002/2017JD026997, 110.

Zhuang, B., Wang, T., Liu, J., Li, S., Xie, M., Han, Y., Chen, P., Hu, Q., Yang, X.Q., Fu, C., Zhu, J., 2017. The surface aerosol optical properties in the urban area of Nanjing, west Yangtze River Delta, China. Atmos. Chem. Phys. 17, 1143–1160. https://doi.org/10.5194/acp-17-1143-2017.